SCIENTIFIC REPORTS
nature research

OPEN

Magnon-tuning non-volatile magnetic dynamics in a CoZr/PMN-PT structure

Cai Zhou[1,3], Ming-fang Zhang[1,3], Fu-fu Liu[2], Ying Jin[2], Chang-jun Jiang[2], Min Hu[1,3], Cun-fang Feng[1,3], Feng-long Wang[4], Ming-yao Xu[1,3]✉ & Sheng-xiang Wang[1,3]✉

Magnon-tuning non-volatile magnetic dynamics is investigated in a CoZr/PMN-PT structure by measuring ferromagnetic resonance at room temperature. The electric-field control of ferromagnetic resonance shows *loop*-like behavior, which indicates non-volatile electric-field control of the magnetism. Further, fitting the curves of in-plane rotating angle versus ferromagnetic resonance field under different electric fields shows that the effective magnetic field changes in *loop*-like manner with the electric field. The resulting change in non-volatile saturation magnetization with electric field is consistent with that of a polarization electric field curve. A 1.04% change of saturation magnetization is obtained, which can be attributed to a magnon-driven magnetoelectric coupling at the CoZr/PMN-PT interface. This magnon-driven magnetoelectric coupling and its dynamic magnetic properties are significant for developing future magnetoelectric devices.

Controlling the electric field in magnetism has the potential to boost spintronics in ferromagnetic/ferroelectric (FM/FE) multiferroic heterostructures[1,2]. In an FM/FE system with interfacial coupling between magnetization and electric polarization, the magnetic dynamics can be mediated by the electric field, in which case the electric field may manipulate the charge carrier density and/or affect the magnetic moment and magnetic anisotropy[3–8]. Further, interfacial charge accumulation or depletion can lead to a non-volatile magnetic response to the electric field[9]. The conventional charge screening length is on the order of an angstrom[10–13]. However, interfacial charge of the FM layer is spin-polarized when the electric field is applied to an itinerant FM layer. A local nonuniform spiral spin density builds up at the interface because the spin-polarization screening charge is surface confined, leading to an initial uniform magnetization away from the interface. This produces a strong and linear magnetoelectric (ME) coupling that is noticeable near the itinerant FM interface. Moreover, the range of spiral spin density can reach the order of nanometers, which has a clear advantage in allowing non-volatile device for information storage. This can be viewed as magnonic accumulation that is stabilized by the charge rearrangement between the coupled FE (with an FE polarization **P**) and FM (with an FM magnetization **M**)[14–20]. Thus, it is predicted that the magnon-driven interfacial ME coupling-induced changes in the magnetic anisotropy will lead to elastic magnetic dynamics in the FM layer. Accordingly, in this work, a polycrystalline CoZr ($Co_{96}Zr_4$) layer is sputtered on a single-crystalline PMN-PT ($Pb(Mg_{1/3}Nb_{2/3})_{0.7}Ti_{0.3}O_3$) substrate through magnetron sputtering. The magnon control of magnetic dynamics in a CoZr/PMN-PT structure is investigated by measuring ferromagnetic resonance (FMR) at room temperature.

Results

Figure 1a shows the out-of-plane θ–2θ XRD scan of the 20-nm CoZr/PMN-PT structure at P^0 state. The term P^0 represents the initial state, in which the crystal is unpolarized. The prominent PMN-PT (011) and (022) peaks are recorded at 31.5° and 65.5°, respectively, which shows the PMN-PT substrate with (011)-orientation[21–23]. The (111) peak of the Pt layer is also present at 39.9°, while there is no CoZr peak in the XRD scans. The phase of the CoZr layer can be considered polycrystalline according to previous work[24]. Remarkably, (011) peak of

[1]Hubei Province Engineering Research Center for Intelligent Micro-Nano Medical Equipment and Key Technologies, Wuhan Textile University, Wuhan 430200, People's Republic of China. [2]Key Laboratory for Magnetism and Magnetic Materials, Ministry of Education, Lanzhou University, Lanzhou 730000, People's Republic of China. [3]Hubei Engineering and Technology Research Center for Functional Fiber Fabrication and Testing, Wuhan Textile University, Wuhan 430200, People's Republic of China. [4]Department of Applied Physics, Chang'an University, Xi'an 710064, People's Republic of China. ✉email: 1988018@wtu.edu.cn; shxwang@wtu.edu.cn

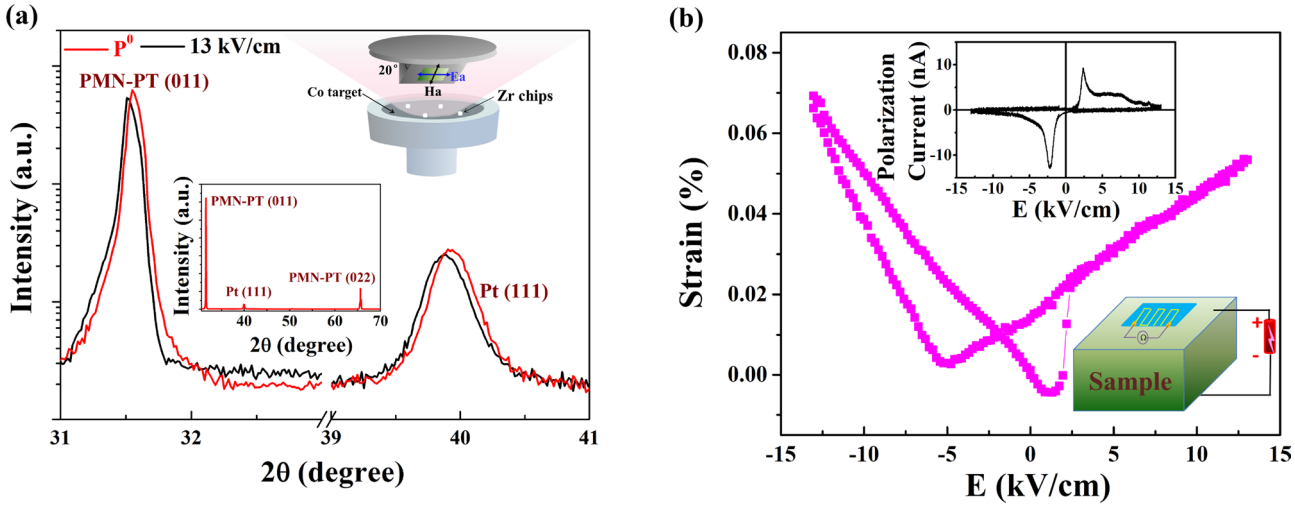

Figure 1. (**a**) XRD 2θ scanning patterns at P^0 state and under the electric field 13.0 kV/cm. The inset shows the schematic of the sputtering arrangement. (**b**) S–E curve. The top inset shows polarization–electric-field curve and thus the electric field tuning of the in-plane polarization current. The bottom inset is a sketch of the strain gauge measurement.

PMN-PT substrate shift toward lower angles under the electric field 13.0 kV/cm, which reveals an expansion along out-of-plane direction. Moreover, a (111) peak of Pt layer also shift toward lower angles, which indicates the PMN-PT substrate produced an out-of-plane tensile strain in the Pt layer associated with applying electric field. The change of out-of-plane lattice parameters of PMN-PT and Pt with application of electric field are estimated as a similar shift of 0.14%[7,22]. The strain was measured with a platform we designed in which the CoZr/PMN-PT structure was stuck on a strain gauge (KFG-A-120-d17, KYOWA) with special glue (CC-33A) as shown in the bottom inset of Fig. 1b. The positive electric field direction was defined as being from top to bottom, whereas negative. The electric field applied on the PMN-PT (011) single-crystalline can produce biaxial in-plane strain. When applying electric field along the [011] direction of PMN-PT, the direction of in-plane compressive stress is along [100] direction of PMN-PT, while the direction of tensile stress is along [01− 1] direction of PMN-PT[25–27]. A *butterfly*-like strain–electric-field (S–E) curve was obtained as shown in Fig. 1b, which is measured along the [01− 1] direction of PMN-PT. The corresponding polarization current curve was shown in the top inset of Fig. 1b, which reveals that the coercive electric field is approximately 2.2 kV/cm. This indicates that the polarization charge can be mediated by the electric field, which leads to the interfacial ME coupling in the CoZr/PMN-PT structure.

The dynamic magnetic property of the CoZr/PMN-PT structure was investigated through FMR measurement at room temperature. Figure 2a shows schematic of the field direction during FMR measurement. Therein, φ is the angle between the direction of the applied magnetic field and the [100] direction of PMN-PT, and ψ is the angle between the direction of magnetization and the [100] direction of PMN-PT. The configuration for FMR spectroscopy is shown in the inset of Fig. 2b. The sample had a 1 mm × 1 mm square shape. Two Cu wires were connected to the top and bottom Pt electrodes of the CoZr/PMN-PT structure, then fixed them by insulating tape. The dc electric field provided by a Keithley 2,410 dc power supply was applied on the two Cu wires. FMR absorption spectra were measured using a lock-in technique based on sweeping a static external magnetic field superimposed over the AC magnetic field. The in-plane rotating-angle FMR integral spectra of the CoZr/PMN-PT structure were obtained for the P^0 state at 0°, 30°, 60° and 90° as shown in Fig. 2b. Because the magnetization was probed using a special phase correlation under the microwave excitation, the spectra in fact correspond to a mixture of imaginary and real parts. Therefore, the actual function of the FMR integral curve is given as[4,16,17]:

$$\zeta(H) = A\frac{\Delta H\cos\delta + (H - H_r)\sin\delta}{\Delta H^2 + (H - H_r)^2} \quad (1)$$

where A is the integral coefficient, ΔH is the half-width at half-maximum, H_r is the magnetic resonance field, δ is the phase that mixes the real and imaginary parts of the dynamic susceptibility, and H is the external magnetic field. The FMR integral curves can be fitted according to the Eq. (1) to obtain related parameters, especially H_r. The H_r–φ curve was obtained for the P^0 state as shown in the top image of Fig. 2c, which demonstrates that the CoZr layer has an in-plane uniaxial anisotropy originating from the oblique magnetron sputtering. At 0° and 180°, H_r is at its minimum, implying the direction of the easy magnetization axis. Meanwhile, the maxima of H_r at 90° and 270° represent the direction of the hard magnetization axis. Similarly, the $H_r - \varphi$ curve under an electric field of 13.0 kV/cm was obtained as shown in the bottom image of Fig. 2c. The directions of the easy and hard magnetization axes remain the same under the applied electric field. However, H_r changes with the electric field, which can be attributed to the interfacial ME coupling in the CoZr/PMN-PT structure.

To investigate the possible interfacial ME coupling, the FMR integral curves under different electric fields were measured at 0° and 90°, respectively. The resulting fitted H_r–E curve is shown in Fig. 3. For the result at

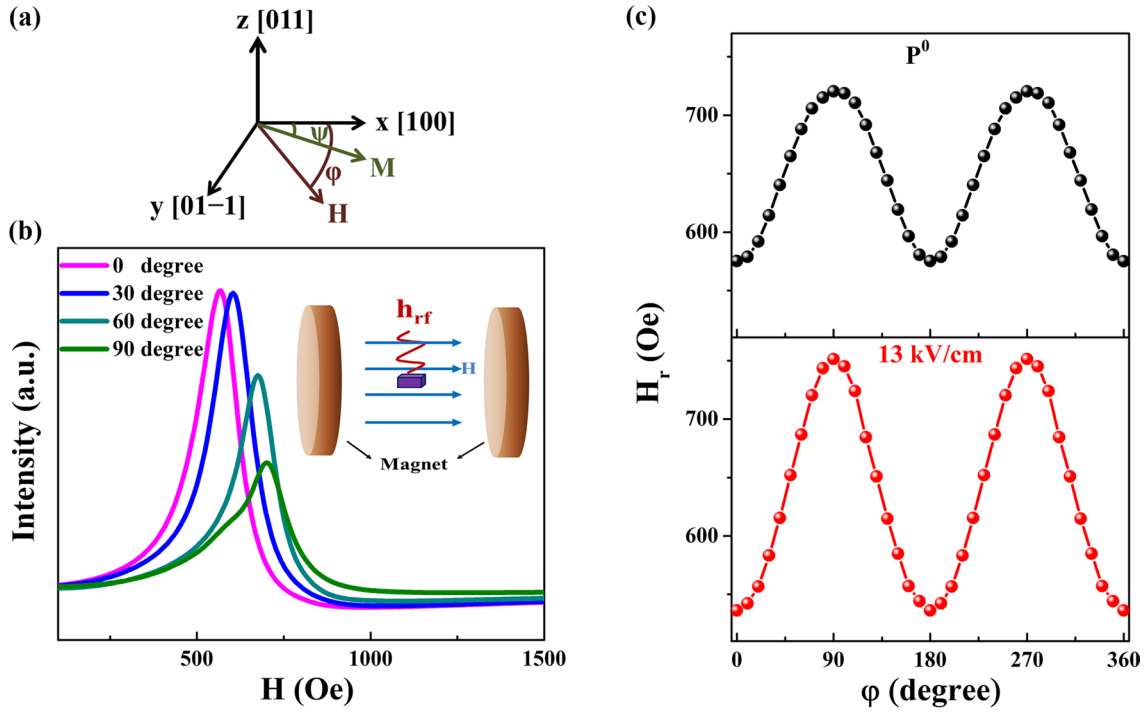

Figure 2. Dynamic magnetic properties at P^0 state and under a electric field of 13.0 kV/cm. FMR integral spectra (**a**) Schematic of field direction during FMR measurement. (**b**) FMR integral spectra with H parallel to the films in-plane at different oblique sputtering angles at P^0 state. The inset shows the configuration for FMR spectroscopy. (**c**) The H_r–φ curves at P^0 state and under an electric field of 13.0 kV/cm.

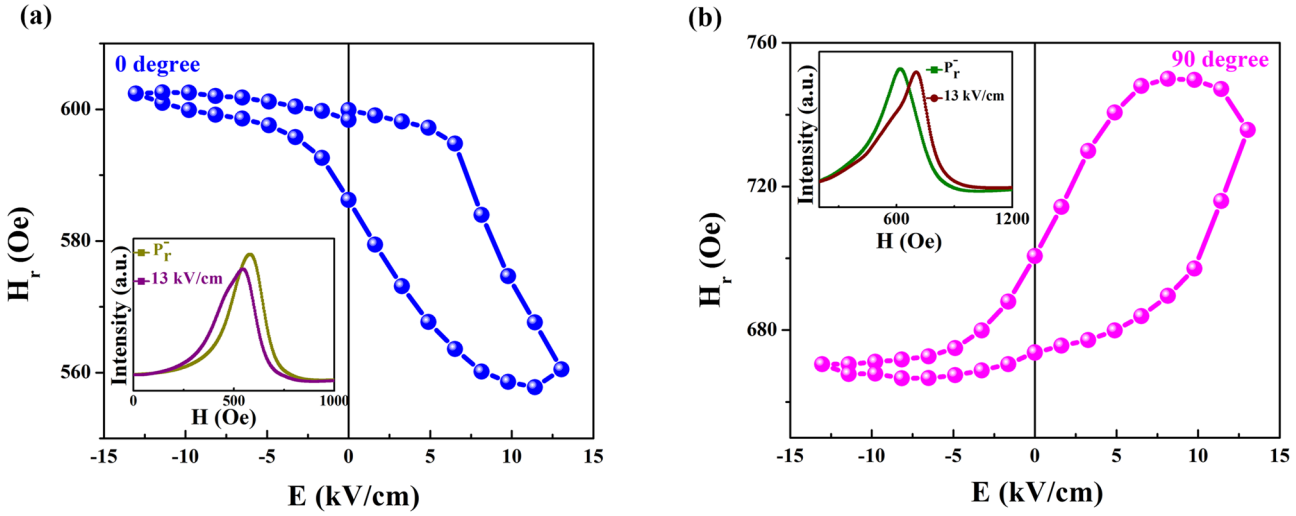

Figure 3. H_r–E curves at 0° and 90°. H_r–E curves at (**a**) 0° and (**b**) 90°. The inset shows the FMR integral spectra at P_r^- state and under an electric field of 13.0 kV/cm.

0° shown in Fig. 3a, the inset shows the FMR integral spectra at P_r^- state and under an electric field of 13.0 kV/cm. The states P_r^+ and P_r^-, are the two remnant polarization states after the applied electric fields of 13.0 and − 13.0 kV/cm are turned off, respectively. Under the positive electric field, H_r decreases sharply when the electric field is swept from the P_r^- state to 13.0 kV/cm, and then increases linearly when the electric field changes from 13.0 kV/cm to the P_r^+ state. Under the negative electric field, the H_r dependence on the electric field from the P_r^+ state to − 13.0 kV/cm slightly increases, and then remains unchanged until the P_r^- state. The *loop*-like H_r–E curve obtained at 0° reveals the non-volatile electric field control of magnetic behavior. Meanwhile, the result at 90° is similar to that in Fig. 3b. There are generally two main ME coupling mechanisms, the piezostrain effect and charge effect, in FM/FE multiferroic heterostructures. The S–E curve for the CoZr/PMN-PT structure in Fig. 1b shows that a piezostrain effect can be transferred to the CoZr layer to achieve a *butterfly*-like magnetic response to the electric field. Compared with the FMR results in Fig. 3, the non-symmetric *loop*-like H_r–E curves

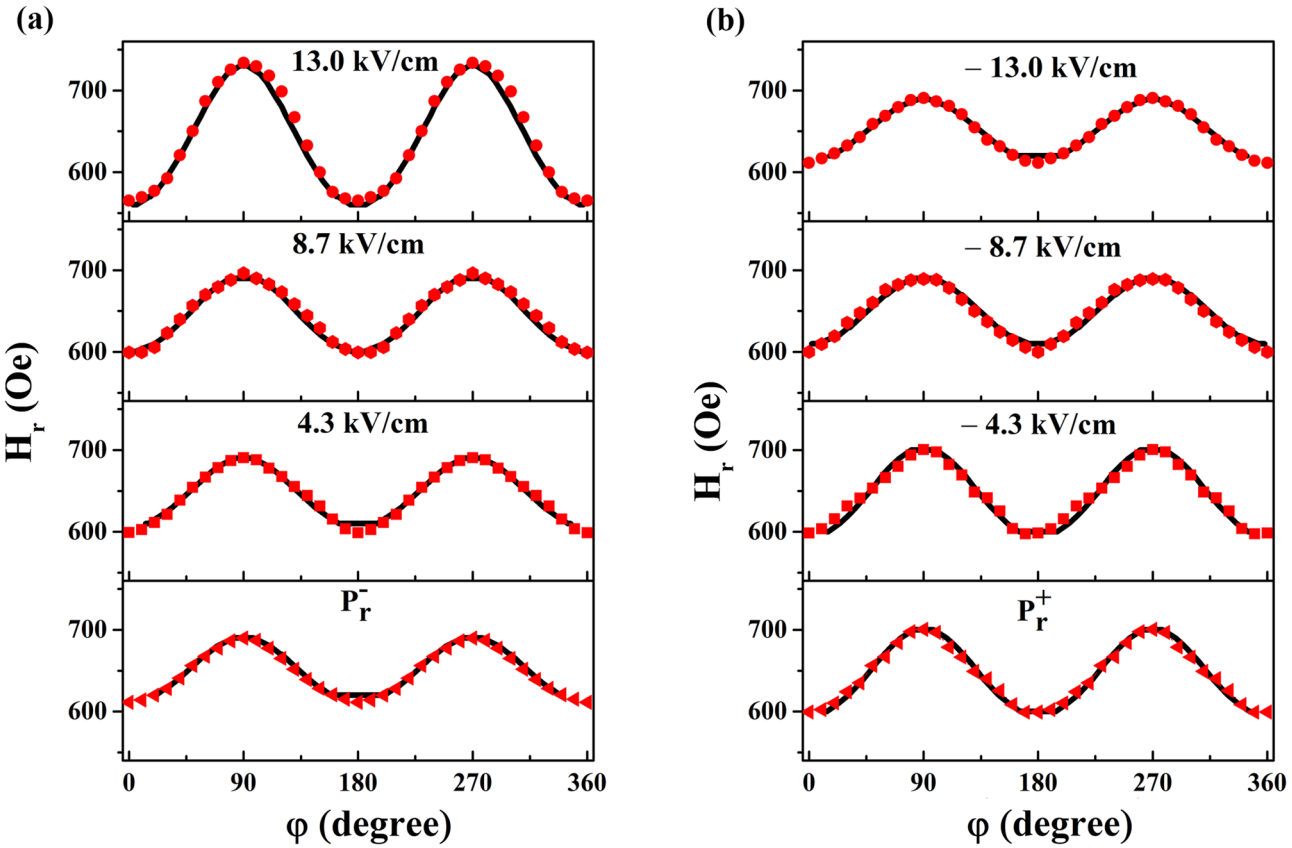

Figure 4. Experimental and fitted H_r–φ curves. Experimental H_r–φ curves (red dots) under (**a**) positive and (**b**) negative electric fields along with the fitted H_r–φ curves (black lines).

demonstrate non-volatile behavior, which is different from the *butterfly*-like S–E curve. This indicates that the piezostrain effect does not play a key role in the interfacial ME effect. The magnetic dynamic result of the coupling phenomena should be considered with care. However, the charge screening length for the conventional charge-mediated mechanism is only a few angstroms. In FeNi/PMN-PT structures and MgO-based magnetic tunnel junctions[10,11], the charge-mediated ME effect is negligible in relatively thick FM layers (≥ 3 nm). Weisheit. et. al. have reported that the magnetocrystalline anisotropy of ordered FePd can be modified by an applied electric field. The strong influence of the surface on the FePd material can be observed only when the thickness of the FePd layer is less than 2 nm[12]. Yi et al. have investigated the charge-modulated ME coupling in a $La_{0.7}Sr_{0.3}MnO_3$/$BiFeO_3$ heterostructure through interface engineering, where the thickness of the $La_{0.7}Sr_{0.3}MnO_3$ layer is only 13 unit cells[28]. The thickness of the CoZr layer in our CoZr/PMN-PT structure is 20 nm, and thus the conventional charge-mediated ME coupling can be ignored, considering that the diffusion length of magnon-driven interfacial ME coupling can reach several tens of nanometers. Moreover, this magnon-driven interfacial ME coupling has a strong correlation between the polarization **P** and magnetization **M** as shown in the top inset of Fig. 5, which leads to a *loop*-like magnetic response to the electric field such as the H_r–E curve as shown in Fig. 3. Therefore, the magnon-driven ME coupling has a predominant effect in the CoZr/PMN-PT structure.

To further verify the magnon-driven interfacial ME coupling in the CoZr/PMN-PT structure, we plot the experimental H_r dependence on φ under different electric fields in Fig. 4 (red dots), which can be fitted using the equation of the in-plane measurement configuration[29]:

$$(\omega/\gamma)^2 = \{H_r\cos(\psi-\varphi) + 4\pi M_s + H_{eff}\cos^2\varphi\}\cdot\{H_r\cos(\psi-\varphi) + H_{eff}\cos 2\varphi\} \quad (2)$$

We take into account magnetization equilibrium:

$$H_r\sin(\psi-\varphi) + H_{eff}\sin\varphi\cos\varphi = 0 \quad (3)$$

where ω is the angular frequency, γ is the gyromagnetic ratio, and H_{eff} is the in-plane effective uniaxial anisotropy field. Figure 4 shows the fitted H_r–φ curves (black lines) based on the experimental H_r–φ curves (red dots). Figures 5 and 6 show the corresponding values of M_s and H_{eff} under different electric fields, respectively.

The *loop*-like dependence of M_s on the electric field is shown in Fig. 5. A 1.04% change of M_s is obtained. This result can be explained as follows: Suppose an FE layer with surface charge σ_{FE} and electric polarization **P** is brought in contact with a charge-neutral FM. The bond rearrangements occur within a few atomic layers of the interface of the FM/FE multiferroic heterostructure, which rearranges spin–polarized charge density *s* on the FM

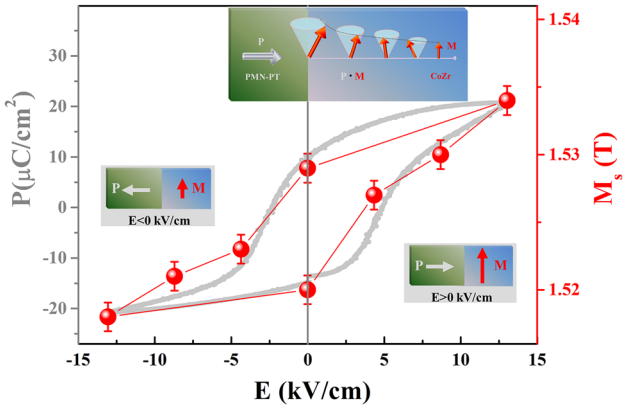

Figure 5. M_s–E and P–E curves. The inset illustrates the P–M interaction.

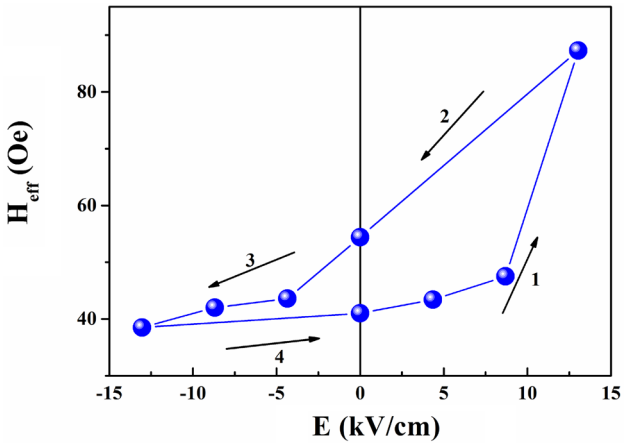

Figure 6. H_{eff}–E curve.

layer. The interfacial spin density can be viewed as a magnonic accumulation stabilized by the **P** of the FE layer at the coupled FE/FM interface, which modifies of the magnitude of the interfacial local magnetic moments. Here we are interested in the interfacial spin density $s_{||}$, whose direction adiabatically follows the intrinsic magnetization **M** at an instant of time, and which is given as: $s_{||}=\eta\sigma_{FE}e^{-z/\lambda}/\lambda$[16–18,20], where η is the spin polarization of the electron density in the CoZr layer in the Stoner mean-field theory, σ_{FE} is the surface charge density, and λ is the effective spin diffusion length in the CoZr layer. Therefore, a major effect on the CoZr layer induced by this magnon-driven ME coupling is the change of the intrinsic magnetization, given as $\Delta M_{||}=\eta\sigma_{FE}\mu_B/d$, with d being the thickness of the CoZr layer. Thus, the *loop*-like M_s–E curve in Fig. 5 is obtained, exhibiting non-volatile behavior, which further magnifies this nonlinear interplay when the sample is measured through FMR. That is, the non-volatile change of intrinsic magnetization can be attributed to the magnon-driven ME coupling, which induces the non-volatile behavior of the H_r–E curve in Fig. 3 and the H_{eff}–E curve in Fig. 6. Moreover, the non-volatile behavior of the *loop*-like M_s–E curve is consistent with that of P–E (polarization–electric-field) curve, which indicates that the magnetization can be modulated by reversing the electric polarization as shown in the left and right insets of Fig. 5.

Experimentally, several reports based on single-crystal (011) PMN-PT, such as $Ni_{0.46}Zn_{0.54}Fe_2O_4$/PMN-PT[7], $Ni_{0.79}Fe_{0.21}$/PMN-PT[13], Fe_3O_4/PMN-PT[22] structure have been investigated, the magnetic properties can be mediated by piezostrain effect due to the piezoelectricity of PMN-PT. To confirm the magnon-driven ME effect rather than the piezostrain effect is a main factor in our system, CoZr thin films with thicknesses 45 nm and 80 nm have been prepared on the PMN-PT substrate in the same sputtering conditions. The result of dynamic measurement can be discussed as following. For the 45-nm-thick CoZr thin film prepared on the PMN-PT substrate, the asymmetric butterfly-like H_r–E curve was shown in Fig. 7a, which was different from the result for 20-nm-thick CoZr thin film. The inset of Fig. 7a showed the FMR integral spectra at P_r^- state and under an electric field of 13.0 kV/cm. In view of the S–E curve as shown in Fig. 1b, the piezostrain effect, derived from PMN-PT substrate, and transferred to the CoZr layer to control the resonance field demonstrating butterfly-like behavior, can be taken into consideration. The behavior of H_r–E curve as shown in Fig. 7a can be regarded as the result of competition between piezostrain and magnon-driven interfacial ME coupling. With increasing the thickness of CoZr thin film to 80 nm, the H_r–E curve was shown in Fig. 7b. The standard butterfly-like curve of the resonance field as

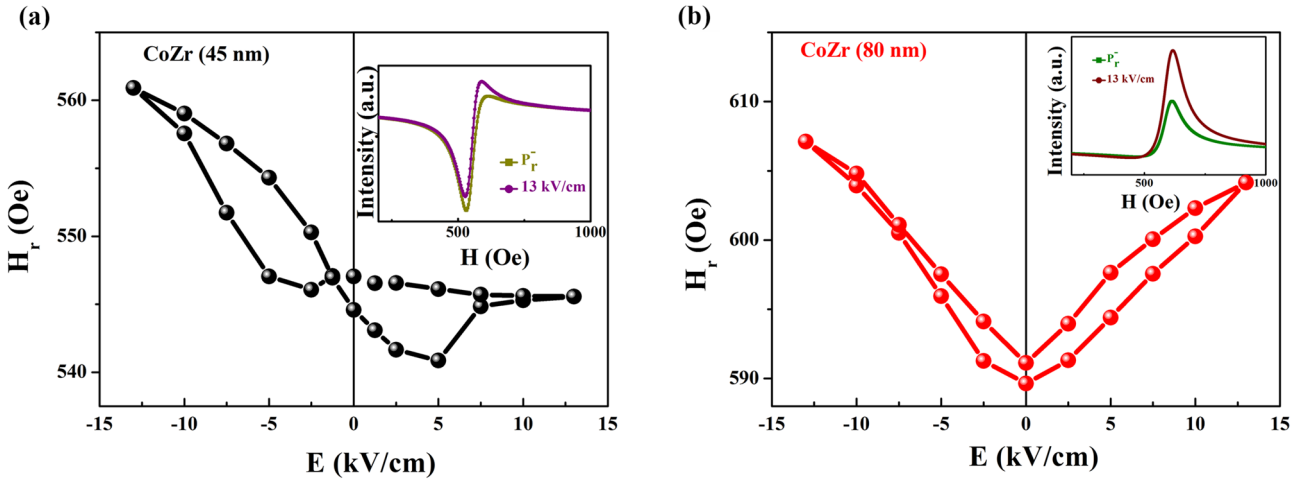

Figure 7. H_r–E curves for CoZr thin film with different thicknesses. (**a**) 45-nm-thick and (**b**) 80-nm-thick CoZr thin film. The insets show the FMR integral spectra at P_r^- state and under an electric field of 13.0 kV/cm.

a function of the electric field was obtained, which was consistent with the result of butterfly-like S–E curve of CoZr/PMN-PT structure as shown in Fig. 1b. The result indicates that the magnetic dynamics of 80-nm-thick CoZr thin film grown on PMN-PT substrate can be mainly mediated by piezostrain effect. However, for the 20-nm-thick CoZr thin film prepared on the PMN-PT substrate, the loop-like H_r–E curve as shown in Fig. 3 exhibits non-volatile behavior, which can be attributed to magnon-driven interfacial ME coupling. The magnon-driven interfacial ME coupling can lead to the non-volatile behavior of nanometer-sized FM layer when applying electric fields. Moreover, the property of respond time of nanoseconds can be widely applied in future microwave devices in GHz frequency band.

Conclusions

We have reported magnon-tuning non-volatile magnetic dynamics in a CoZr/PMN-PT structure. A *loop*-like curve was obtained for the resonance field versus electric field, exhibiting non-volatile behavior. This can be attributed to the magnon-driven interfacial magnetoelectric coupling. We fitted the experimental results for the resonance field versus in-plane rotating-angle under different electric fields, and obtained a *loop*-like magnetization response to the electric field. This further verifies that the magnon-driven interfacial magnetoelectric coupling has a dominant role in the CoZr/PMN-PT structure, which leads to the resulting *loop*-like curve of the effective magnetic field versus electric field. This can be applied in spintronic devices with new functions.

Methods

Sample preparation. The polycrystalline CoZr thin film was deposited through radio-frequency (RF) magnetron sputtering with an oblique sputtering angle of 20° on a 230-μm-thickness single-crystal (011) PMN-PT substrate. As shown in the inset of Fig. 1a, four Zr chips were regularly placed on a Co target, and the composition of the deposited magnetic layer was adjusted by controlling the number of Zr chips. The thickness of the CoZr film was 20 nm. The easy axis of the CoZr thin film during sputtering was along the [100] direction of the PMN-PT substrate. Pt layers with thicknesses of 20 nm and 100 nm were sputtered on the top and bottom surfaces to act as electrodes, respectively. Cu wires were then connected to the electrodes.

Measurement. A biased voltage was applied a Keithley 2,410 dc power supply through the Cu wires connected to the electrodes. FMR measurements were performed using a JEOL JES-FA 300 spectrometer (power of 1 mW, X-band at 8.969 GHz). The electromagnet is used to provide a static external magnetic field. At the center of the electromagnet, a cylindrical cavity resonator is set to put sample into it. The microwave is generated by waveguide connected with the cylindrical cavity resonator, which is normal to the sample. This microwave unit can also detect the reflection. X-ray diffraction (XRD) was measured with an X'Pert X-ray powder diffractometer with Cu K_α radiation (1.54056 Å). Using a Sawyer Tower circuit, the hysteresis polarization–electric-field loop was taken with a computer interfaced-loop-tracer.

Received: 28 May 2020; Accepted: 12 August 2020
Published online: 01 September 2020

References

1. Spaldin, N. A. & Ramesh, R. Advances in magnetoelectric multiferroics. *Nat. Mater.* **18**, 203–212 (2019).
2. Sun, N. Multiferroics and the path to the market. *Nat. Mater.* **18**, 191–192 (2019).
3. Wang, W. Q. *et al.* Temperature dependence of interlayer exchange coupling and Gilbert damping in synthetic antiferromagnetic trilayers investigated using broadband ferromagnetic resonance. *Appl. Phys. Lett.* **113**, 042401 (2018).
4. Zhou, C., Dunzhu, G. S., Yao, J. L. & Jiang, C. J. Piezostrain control of magnetic anisotropy in $Co_2FeAl/Pb(Mg_{1/3}Nb_{2/3})O_3$–30%$PbTiO_3$ heterostructure. *J. Alloy. Compd.* **710**, 680 (2017).

5. Zhou, C., Zhang, C., Yao, J. L. & Jiang, C. J. Lateral electric-field-driven non-volatile four-state memory in multiferroic heterostructures. *Appl. Phys. Lett.* **109**, 112404 (2016).
6. Zhou, C., Wu, L., Zhang, C., Yao, J. L. & Jiang, C. J. Electric field tuning resistance switching behavior of $SrRuO_3$/Pb($Mg_{1/3}Nb_{2/3}$)O_3–$PbTiO_3$ heterostructures at various temperatures. *J. Phys. D Appl. Phys.* **49**, 425003 (2016) (**6pp**).
7. Dong, C. H. *et al.* Piezoelectric control of magnetic anisotropy in the $Ni_{0.46}Zn_{0.54}Fe_2O_4$/Pb($Mg_{1/3}Nb_{2/3}$)$O_3$–$PbTiO_3$ composite. *Appl. Phys. Lett.* **104**, 062403 (2014).
8. Wang, F. L. *et al.* Piezoelectric control of magnetic dynamics in Co/Pb($Mg_{1/3}Nb_{2/3}$)O_3-$PbTiO_3$ heterostructure. *Appl. Phys. Lett.* **105**, 062407 (2014).
9. Molegraaf, H. J. A. *et al.* Magnetoelectric effects in complex oxides with competing ground states. *Adv. Mater.* **21**, 3470 (2009).
10. Wang, W. G., Li, M. G., Hageman, S. & Chien, C. L. Electric-firld-assisted switching in magnetic tunnel junctions. *Nat. Mater.* **11**, 64 (2012).
11. Shiota, Y. *et al.* Induction of coherent magnetization switching in a few atomic layers of FeCo using voltage pulses. *Nat. Mater.* **11**, 39 (2012).
12. Weisheit, M. *et al.* Electric field-induced modification of magnetism in thin-film ferromagnets. *Science* **315**, 349 (2007).
13. Nan, T. X. *et al.* Quantification of strain and charge co-mediated magnetoelectric coupling on ultra-thin Permalloy/PMN-PT interface. *Sci. Rep.* **4**, 3688 (2014).
14. Lebrun, R. *et al.* Tunable long-distance spin transport in a crystalline antiferromagnetic iron oxide. *Nature* **561**, 222–238 (2018).
15. Jiang, C. J., Jia, C. L., Wang, F. L., Zhou, C. & Xue, D. S. Transformable ferroelectric control of dynamic magnetic permeability. *Phys. Rev. B* **97**, 060408(R) (2018).
16. Zhou, C. *et al.* Long-range non-volatile electric field effect in epitaxial Fe/Pb($Mg_{1/3}Nb_{2/3}$)$_{0.7}Ti_{0.3}O_3$ heterostructure. *Adv. Funct. Mater.* **28**, 1707027 (2018).
17. Zhou, C. *et al.* Strong non-volatile magnon-driven magnetoelectric coupling in single crystal Co/PMN-PT(001) heterostructures. *Phys. Rev. Appl.* **9**, 014006 (2018).
18. Li, Y. J., Chen, M., Berakdar, J. & Jia, C. L. Gate-controlled magnon-assisted switching of magnetization in ferroelectric/ferromagnetic junctions. *Phys. Rev. B* **96**, 054444 (2017).
19. Cornelissen, L. J., Liu, J., Duine, R. A., Youssef, J. B. & van Wees, B. J. Long-distance transport of magnon spin information in a magnetic insulator at room temperature. *Nat. Phys.* **11**(12), 1022–1026 (2015).
20. Jia, C. L. *et al.* Mechanism of interfacial magnetoelectric coupling in composite multiferroics. *Phys. Rev. B* **90**, 054423 (2014).
21. Wu, T. *et al.* Carman. Domain engineered switchable strain states in ferroelectric (011)[Pb($Mg_{1/3}Nb_{2/3}$)O_3]$_{(1-x)}$-[$PbTiO_3$]$_x$ (PMN-PT, x ≈ 032) single crystals. *J. Appl. Phys.* **109**, 124101 (2011).
22. Liu, M. *et al.* Non-volatile ferroelastic switching of the Verwey transition and resistivity of epitaxial Fe_3O_4/PMN-PT (011). *Sci. Rep.* **3**, 1876 (2013).
23. Nan, T. X., Liu, M., Ren, W., Ye, Z. G. & Sun, N. X. Voltage control of metal-insulator transition and non-volatile ferroelastic switching of resistance in VO_x/PMN-PT heterostructures. *Sci. Rep.* **4**, 5931 (2014).
24. Jia, C. L., Wang, F. L., Jiang, C. J., Berakdar, J. & Xue, D. S. Electric tuning of magnetization dynamics and electric field-induced negative magnetic permeability in nanoscale composite multiferroic. *Sci. Rep.* **5**, 11111 (2015).
25. Chen, A. T. *et al.* Giant nonvolatile manipulation of magnetoresistance in magnetic tunnel junctions by electric fields via magnetoelectric coupling. *Nat. Commun.* **10**, 243 (2019).
26. Liu, M. *et al.* Giant electric field tuning of magnetic properties in multiferroic ferrite/ferroelectric heterostructures. *Adv. Funct. Mater.* **19**, 1826 (2009).
27. Wang, Z., Wang, Y., Ge, W., Li, J. & Viehland, D. Volatile and nonvolatile magnetic easy-axis rotation in epitaxial ferromagnetic thin films on ferroelectric single crystal substrates. *Appl. Phys. Lett.* **103**, 132909 (2013).
28. Yi, D. *et al.* Tailoring magnetoelectric coupling in $BiFeO_3$/$La_{0.7}Sr_{0.3}MnO_3$ heterostructure through the interface engineering. *Adv. Mater.* **31**(11), 1806335 (2019).
29. Zhou, C., Wang, F. L., Dunzhu, G. S., Yao, J. L. & Jiang, C. J. Piezostrain tuning non-volatile 90° magnetic easy axis rotation in Co_2FeAl Heusler alloy film grown on Pb($Mg_{1/3}Nb_{2/3}$)O_3-$PbTiO_3$ heterostructures. *J. Phys. D: Appl. Phys.* **49**, 455001 (2016) (**6pp**).

Acknowledgements

This work is supported by the National Natural Science Foundation of China (Grant Nos. 51671099, 11974149 and 51901163); the Foundation of Wuhan Textile University (Grant No. 193128).

Author contributions

M.Y.X., S.X.W. designed the experiments. C.Z., F.L.W performed the experiments. C.Z., M.F.Z., C.F.F., F.F.L., Y.J., C.J.J. and M.H. analyzed the results. All authors reviewed the manuscript.

Competing interests

The authors declare no competing interests.

Additional information

Correspondence and requests for materials should be addressed to M.X. or S.W.

Reprints and permissions information is available at www.nature.com/reprints.

Publisher's note Springer Nature remains neutral with regard to jurisdictional claims in published maps and institutional affiliations.